nature communications

Article

https://doi.org/10.1038/s41467-024-53304-3

Advanced nanobubble flotation for enhanced removal of sub-10 μm microplastics from wastewater

Received: 3 February 2024

Accepted: 9 October 2024

Published online: 21 October 2024

Check for updates

Mingyi Jia[1], Muhammad Usman Farid[1,2] ✉, Yuen-Wa Ho[3], Xinyao Ma[4], Pak Wai Wong[1], Theodora Nah[1,5], Yuhe He[1,5], Min Wei Boey[1], Gang Lu[1], James Kar-Hei Fang[3,5], Jun Fan[4] & Alicia Kyoungjin An[1,2] ✉

Sub-10 μm microplastics (MPs) in aquatic environments pose significant ecological and health risks due to their mobility and potential to carry harmful microcontaminants. Our effluent analysis from a Hong Kong Sewage Treatment Works shows that traditional treatment often fails to effectively remove these MPs. These small-sized MPs are commonly neglected due to challenges in accurate quantification, analysis, and removal. This study introduces a nanobubble-assisted flotation process that enhances the removal efficiency of both regular and irregular small-sized MPs from wastewater. The proposed process outperforms the traditional flotation process by fostering a more effective interaction between bubbles and MPs, increasing removal rates of MPs from 1 μm to 10 μm by up to 12% and providing a total efficiency boost of up to 17% for various particle sizes. Improvements are attributed to enhanced collision and adhesion probabilities, hydrophobic interactions, as well as better floc flotation. Supported by empirical evidence, mathematical models, and Molecular Dynamics simulations, this research elucidates the nanoscale mechanisms at play. The findings confirm the nanobubble-assisted flotation technique as an innovative and practical approach to removing sub-10 μm MPs in water treatment processes.

The occurrence, transport, and distribution of microplastics (MPs) and their removal strategies have been extensively investigated on a global scale due to their wide distribution and ecotoxic effects[1]. It has been reported that in water matrices, the abundance of MPs increases by 1.6 to 7.9 times with every tenfold reduction in particle size[2]. Wastewater treatment plants are considered one of the primary point sources of MP discharge, particularly for those in the smaller size range (<100 μm) that are not effectively separated by conventional pretreatment, primary, and secondary treatment processes and are dominant in the effluent[3]. The ecotoxicological impact of small-sized MPs is of more significant concern due to their higher likelihood of ingestion by aquatic organisms and their higher surface area-to-volume ratio, which renders them efficient carriers of micropollutants and pathogens[4,5]. Studies have shown that mussels can ingest MPs ranging from 3 to 10 μm, and crabs can take up spherical MPs of 8 to 10 μm in size through feeding or inspiration across their gills[6,7]. Consequently, there is a growing interest in developing more effective treatment processes to enhance the removal of small-sized MPs from wastewater[8–10].

[1]School of Energy and Environment, City University of Hong Kong, Tat Chee Avenue, Kowloon, Hong Kong SAR, China. [2]Department of Chemical and Biological Engineering, The Hong Kong University of Science and Technology, Clear Water Bay, Kowloon, Hong Kong SAR, China. [3]Department of Food Science and Nutrition, The Hong Kong Polytechnic University, Yuk Choi Road, Kowloon, Hong Kong SAR, China. [4]Department of Materials Science and Engineering, City University of Hong Kong, Kowloon, Hong Kong SAR, China. [5]State Key Laboratory of Marine Pollution, City University of Hong Kong SAR, Tat Chee Avenue, Kowloon, Hong Kong, China. ✉e-mail: mufarid@ust.hk; alicia.kjan@ust.hk

Flotation, a commonly applied separation technique in water treatment, has been identified as a promising treatment process for removing MPs[11–13]. While this process effectively removes suspended particles within the 50–150 μm size range, it struggles with fine and coarse particles outside this range[14]. Prior research on flotation processes, summarized in Supplementary Table 1, confirms their efficacy in removing larger-sized MPs, though these studies generally overlook the smaller-sized MPs. For instance, a study reported that a full-scale flotation system, pretreated with 40 mg L^{-1} polyaluminium chloride, achieved a 95% removal efficiency of MPs larger than 20 μm using grab sampling, and 48% using 24-h composite sampling[8]. Another study, utilizing a lab-scale dissolved air flotation jar tester, found MPs removal efficiencies of less than 35% for 2–5 μm, 45% for 5–10 μm, and 85% for 15–20 μm MPs, suggesting that the technique is not as successful in recovering small-sized MPs[15].

The efficiency of the flotation process, primarily driven by bubble-particle interactions, can be improved by increasing particle size with coagulants/flocculants or by decreasing bubble size through modifications in the bubble generation process or addition of surfactants[16,17] Nanobubbles (NBs), defined as bubbles with sizes less than 1000 nm, have been increasingly researched in various fields due to their unique properties, which include miniature size, high concentration, and high stability[18–20]. NBs' higher surface area-to-volume ratio and high concentration can increase the probability of collision and adhesion with fine particles[21–23]. Moreover, by attaching to particles, NBs can increase the contact angle of fine particles and reduce the probability of their detachment from bigger bubble[24,25]. Meanwhile, the low rising velocity of NBs, which endows long stability and residence time in the contact zone, also minimizes the air loss due to rapid bubble burst/rise[26]. Interestingly, given these properties, NBs have been reported to enhance the separation of oil droplets and amine precipitates, and to recover mineral particles in froth flotation[27–29]. Yet, whether NBs can assist with enhancing MPs removal in wastewater remains unknown.

In response to the significant challenge of removing small-sized MPs during wastewater treatment, this study introduces an approach that specifically targets the effective removal of small-sized MPs ranging from 1 to 50 μm by combining NBs to the existing microbubble flotation (MB-F) process and utilizing varying concentrations of aluminum chloride ($AlCl_3$) coagulant (5–25 ppm). The efficacy of this combined micro-nanobubble flotation (MNB-F) technique was tested in both synthetic and real wastewater environments and compared with nanobubble flotation (NB-F) and traditional MB-F. Recognizing the intricate challenges of understanding particle-bubble interactions due to the small sizes of MPs and NBs, numerical flotation models and Molecular Dynamics (MD) simulations were employed in this work to elucidate the underlying mechanisms for enhanced flotation processes from a micro and nanoscopic perspective. Additionally, we evaluated the reactivity of NBs in water and compared the concurrent removal of total organic carbon (TOC) from wastewater using MB-F and MNB-F. Both the experimental and simulation results provide compelling evidence that NBs play a meaningful role in enhancing existing flotation processes. By offering an improvement over existing technologies, this study holds considerable practical significance for wastewater treatment facilities aiming to reduce MPs pollution more effectively.

Results and discussion

Evaluating the prevalence of small-sized MPs in real-wastewater environments

Characterizing MPs, particularly those of smaller sizes, is challenging and often neglected, leading to a scarcity of data on their distribution in water bodies[30]. A few studies conducted on the size distribution of MPs in the influents and effluents of wastewater have reported that large MPs are more easily removed, leaving primarily small-sized MPs in the effluent (Fig. 1a). The observed limited efficiency in removing small-sized MPs suggests that a significant quantity of these particles continues to be released into natural water bodies.

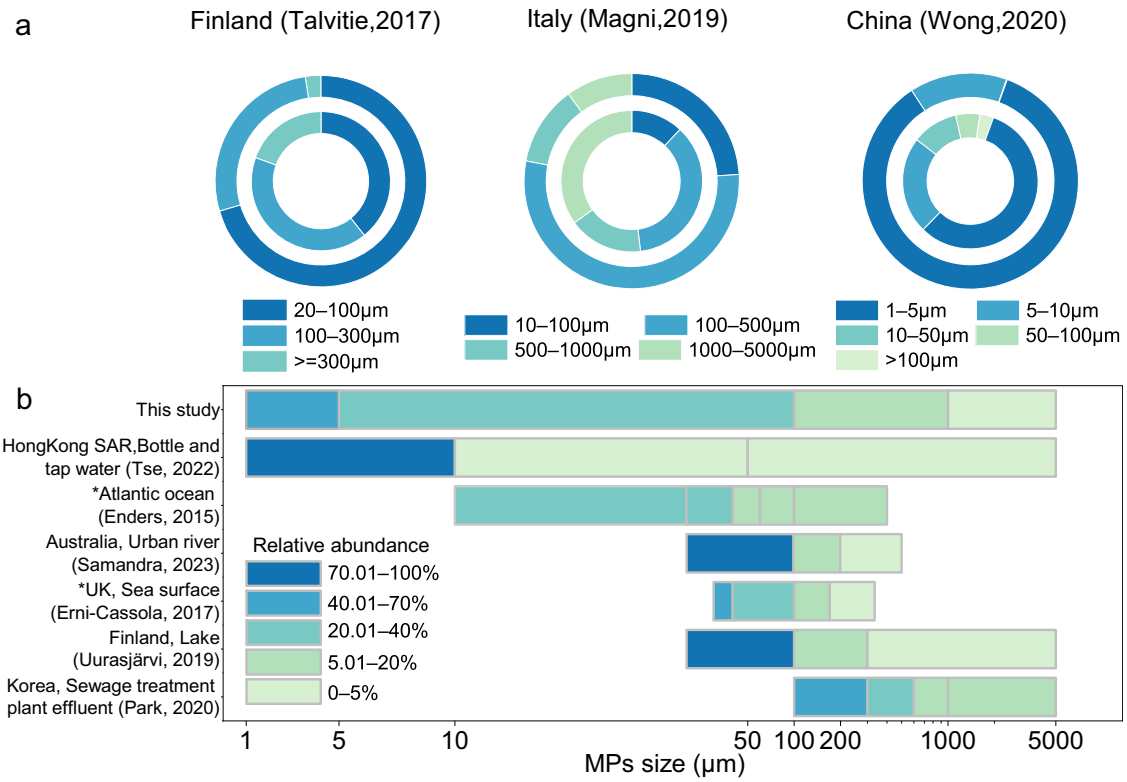

Fig. 1 | MP size distributions in various water matrices around the globe. **a** Percentage composition of MPs in the influent (inner circle) and effluent (outer circle) of wastewater treatment facilities worldwide. **b** Size distribution of MPs in surface water locations globally. *Data extracted from figures in referenced studies using WebPlotDigitizer.v.4.8[85].

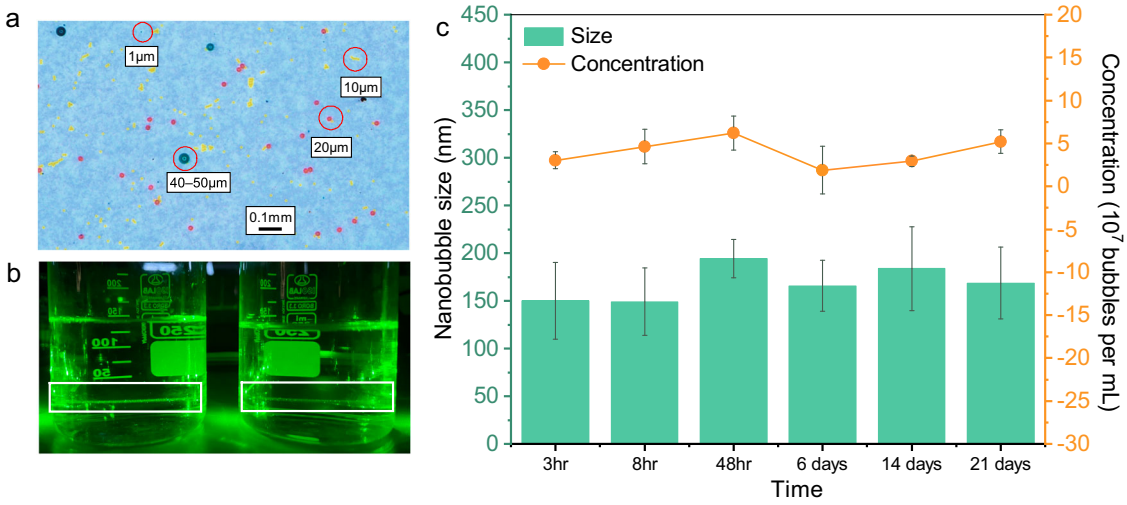

Fig. 2 | Visualization and characterization of NBs in DI water. a PS MPs under microscopy, with different sizes color-coded: Green for 40–50 μm; Orange for 20 μm; Yellow for 10 μm; Blue for 1 μm. Red circles highlight examples of MPs of various sizes. **b** Differentiation of DI water from NB water by dynamic light scattering, using a green laser pointer, as indicated by the white rectangle. **c** Changes in NBs' size and concentration over 21 days. Data points and error bars represent the mean and standard deviation of three measurements.

We performed a preliminary analysis of MPs concentrations and sizes to determine the size distribution of MPs in the effluent of a Hong Kong Sewage Treatment Work after chemically enhanced primary treatment (an additional step of coagulation and sedimentation after primary treatment). A Raman microscope was used to identify MPs larger than 5 μm, and an Optical Photothermal Infrared (O-PTIR) spectroscopy system was used to quantify MP particles between 1–5 μm. Selected spectra from the O-PTIR and Raman analyses are presented in Supplementary Fig. 1a–d. After quantifying three subsamples, we obtained an average of 25.67 ± 8.33 particles per 100 mL of the sample for MPs larger than 5 μm and an average of 204.53 ± 73.06 particles per 100 mL of the sample for MPs in the range of 1–5 μm in the effluent (Supplementary Fig. 1e). Similar to previous studies, which noted a pattern where the abundance of MPs increases with the decrease in particle size in various aquatic environments, this study also found a higher number of MPs in the smaller size range (Fig. 1b)[31–39]. The characterization results emphasize the urgent need to enhance the removal of small-sized MPs during water treatment processes.

Characterizing the physicochemical properties of commercial MPs and NBs

The sizes and polymer types of the purchased MPs were verified using a stereomicroscope, a field emission scanning electron microscope (FE-SEM), and a Fourier transform infrared (FT- IR) spectrometer (Fig. 2a and Supplementary Figs. 2–4). Given the importance of bubble sizes and concentrations in flotation processes, we first determined the properties of the bubbles generated during flotation. As MB-F is a well-established treatment process, extensive research has been conducted on the sizes and distribution of bubbles generated during MB-F, reporting sizes generally ranging from 20 to 100 μm and a bubble concentration of 10^4 bubbles mL^{-1} [40–42]. On the other hand, NBs are yet an emerging area of research, and the fundamental characteristics of NBs remain to be confirmed. After generating NBs using the hydrodynamic cavitation method, the presence of NBs was verified using a laser beam, which can differentiate between NB-water and DI-water based on the Tyndall effect (Fig. 2b). The hydrodynamic cavitation method, commonly used in various studies and commercial applications, generates NBs consistently with high concentrations, stability, and small sizes[43].

Next, the generated NB water was analyzed to determine the average bubble size, concentration, and stability over 21 days (Fig. 2c). The results revealed that the average bubble concentration is approximately 3.04×10^7 bubbles per mL, with bubble diameters ranging from 100 to 150 nm. These measurements of size, concentration, and stability of NBs in line with those reported in existing literature, where generated NBs are reported to persist for over a month with sizes ranging from 100 to 200 nm and concentrations ranging from 10^6 to 10^8 [19,20,44]. Furthermore, the zeta potential of the NBs, measured immediately after generation, was around −16 mV at neutral pH, consistent with typical values (−50 to −20 mV under different conditions)[45], indicating their stability due to the repulsive forces between the bubbles.

Exploring NBs contributions to MP removal by flotation

Comparative analysis of three flotation techniques: MB-F, MNB-F, and NB-F. To investigate the role of NBs in flotation and determine whether NB flotation can function as a stand-alone technique, we conducted a comparative study involving three flotation techniques: MB-F, MNB-F, and NB-F. The aim was to assess their efficiencies in removing spherical polystyrene (PS) MPs of two different sizes at an $AlCl_3$ dosage of 10 ppm in synthetic wastewater. Experimental results demonstrated that, for MPs sized 40–50 μm, both MB-F and MNB-F achieved a removal efficiency of over 90%, while NB-F only removed 77.1% (independent *t*-test, $p < 0.05$). Similarly, for MPs sized 20 μm, MB-F and MNB-F exhibited an overall removal efficiency of approximately 80%, whereas NB-F only removed 69.5% (Fig. 3a). For both sizes of MPs, there was no significant difference in removal efficiency between MB-F and MNB-F (independent *t*-test, $p > 0.05$). At the same time, NB-F showed a significantly lower removal efficiency in comparison (independent *t*-test, $p < 0.05$).

The lower removal efficiency observed in NB-F can be attributed to the predominance of NBs during flotation, which have limited lifting force or rising velocity to transport particles and flocs to the water surface[22]. Numerical models are employed to further investigate the impact of bubble sizes in the micrometer and nanometer range on rising velocity. We considered the commonly reported size distributions for MBs and NBs for the modeling: from 20 μm to 100 μm for MBs, with the highest intensity occurring at 65 μm[40–42], and from 100 nm to 1000 nm for NBs, with the highest intensity occurring at around 300 nm[19,20].

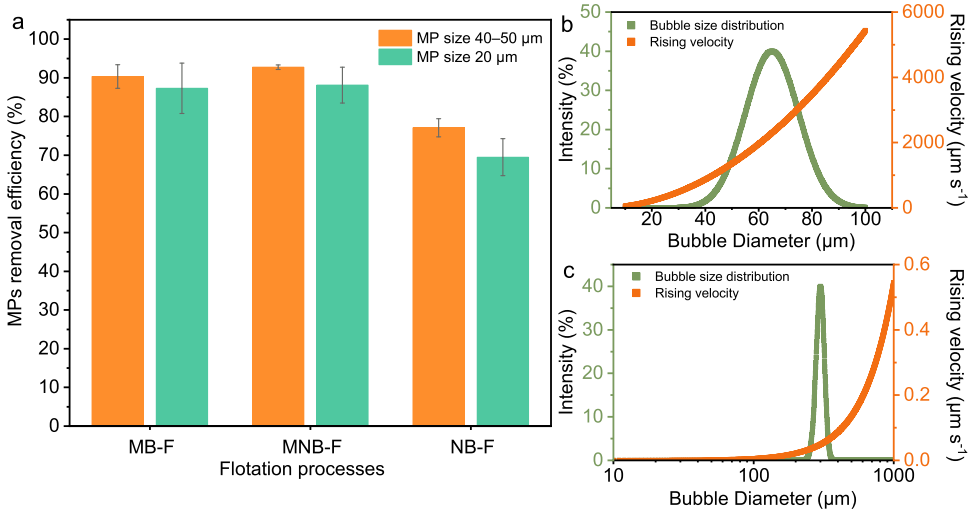

Fig. 3 | Removal of MPs using bubbles of varying sizes and rising velocities. **a** MPs removal efficiency of the three flotation processes (MB-F, MNB-F, and NB-F) at an $AlCl_3$ dosage of 10 ppm. **b** Bubble size distribution and their theoretical rising velocity in MB-F. **c** Bubble size distribution and their theoretical rising velocity in NB-F. Data points and error bars represent the mean and standard deviation from two independent experiments.

For NBs with small bubble sizes and low Reynolds (Re) numbers, Stokes' law was employed (Eq. (2)). For MBs (>10 μm) with larger Re numbers, the Hadamard-Rybczynski equation (Eq. (3)) was utilized as suggested in previous research[46]. The mathematical modeling approach provides a clear demonstration of how bubble size influences their rising velocity, offering insights into the differing performances of NB-F and MB-F in terms of flotation efficiency[46,47]:

$$\mathrm{Re} = \frac{\rho_s U d_b}{\mu} \tag{1}$$

$$U_{\mathrm{Stoke}} = \frac{2}{9} \times \frac{\rho_s - \rho_w}{\mu} \times g \times {r_b}^2 \tag{2}$$

$$U_{H-R} = \frac{3}{2} \times \frac{2}{9} \times \frac{\rho_s - \rho_w}{\mu} \times g \times {r_b}^2 \tag{3}$$

where U is the bubble terminal rising velocity, ρ_s is the density of the bubble sphere ($g\,\mu m^{-3}$), d_b is bubble diameter (μm), r_b is the bubble diameter distribution (μm), ρ_w is the water density ($g\,\mu m^{-3}$), μ is the dynamic viscosity ($g\,(\mu m\,s)^{-1}$), g is the gravity ($\mu m\,s^{-2}$). The parameter values used are provided in Supplementary Table 2.

As shown in Fig. 3b, c, the modeled results revealed that MBs with radii ranging from 20–100 μm can achieve a maximum rising velocity of around 6000 μm^{-s}. On the other hand, NBs with sizes ranging from 10–1000 nm exhibit about ten thousand times lower rising velocity than MBs. Due to NBs' low rising velocity, NB-F cannot function as a stand-alone technique for flotation, necessitating its combination with coarse bubbles (macro bubbles and MBs) to enhance flotation efficiency.

Evaluating the removal efficiency of MPs across four sizes with two quantitative approaches. To address the challenge of accurately and efficiently quantifying small-sized MPs, two MPs quantification methods were evaluated prior to removal tests: an indirect technique that measures the turbidity of the solution, and a direct method that involves filtering MPs onto filter paper and analyzing their area coverage under a microscope through image analysis. Figure 4a depicts a linear relationship between turbidity and concentration for 1 μm and 10 μm PS MPs ($R^2 = 0.99$ for 1 μm, $R^2 = 0.98$ for 10 μm), contrasting with the less linear relationships observed for 20 μm and 40–50 μm PS MPs (Fig. 4b, $R^2 = 0.95$ for 20 μm, $R^2 = 0.91$ for 40–50 μm). Our results suggest that turbidity can serve as a relatively accurate indicator for determining the concentration of 1–10 μm MPs in water, which aligns with a previous study that reported an R^2 value greater than 0.99 when analyzing the correlation between turbidity and concentration for 0.1 μm, 1 μm, and 10 μm PS MPs[48]. Another study reported a low correlation between pristine PE MPs and turbidity, where the correlation coefficients for 140 μm and 15 μm PE were 0.42 and 0.71, respectively[49]. The image analysis method, on the other hand, yielded good accuracy with linear relationships observed for 10 μm, 20 μm, and 40–50 μm MPs with R-squared all larger than 0.99 (Fig. 4c).

We then used the two methods to quantify the simultaneous removal of a mixture of four different-sized PS MPs in synthetic wastewater using MB-F and MNB-F processes and compared the results. It was found that irrespective of the quantification methods employed, MNB-F achieved a higher cumulative removal of MPs than MB-F, suggesting that NBs can play a role during the flotation process (Fig. 4d). When comparing the two quantification methods with the removal results, the image analysis method showed a statistically significant difference (independent t-test, $p < 0.05$) with a 16.8% disparity in MPs removal efficiencies between MNB-F and MB-F. In contrast, the turbidity method revealed an insignificant difference of about 8.4% (independent t-test, $p = 0.064$). The primary reason for this notable difference between the two quantification methods can be attributed to the ineffectiveness of the turbidity method in detecting the presence of larger MPs, which have a lower particle count per mL and are less evenly distributed in the water[48]. Consequently, subsequent analyses in this study employed the image analysis method to determine the removal of larger particles (10–50 μm) and the turbidity method for measuring the removal of <10 μm particles.

Building upon the above analyses, a systematic investigation was undertaken to explore the factors contributing to the improved removal of MPs. Specifically, we evaluated the impacts of MPs' sizes, shapes, and polymer types, as well as the various concentrations of $AlCl_3$ on flotation efficiency.

Assessing the role of particle and floc sizes in small-sized MP removal processes. First, we evaluated the removal efficiency of spherical PS MPs in the sizes of 1 μm, 10 μm, 20 μm, and 40–50 μm under three different coagulant dosages, i.e., 5, 10, 25 ppm in synthetic wastewater (Fig. 5). In the flotation process, the coagulant dosages can vary significantly, ranging from 5 to 500 $mg\,L^{-1}$, depending on the

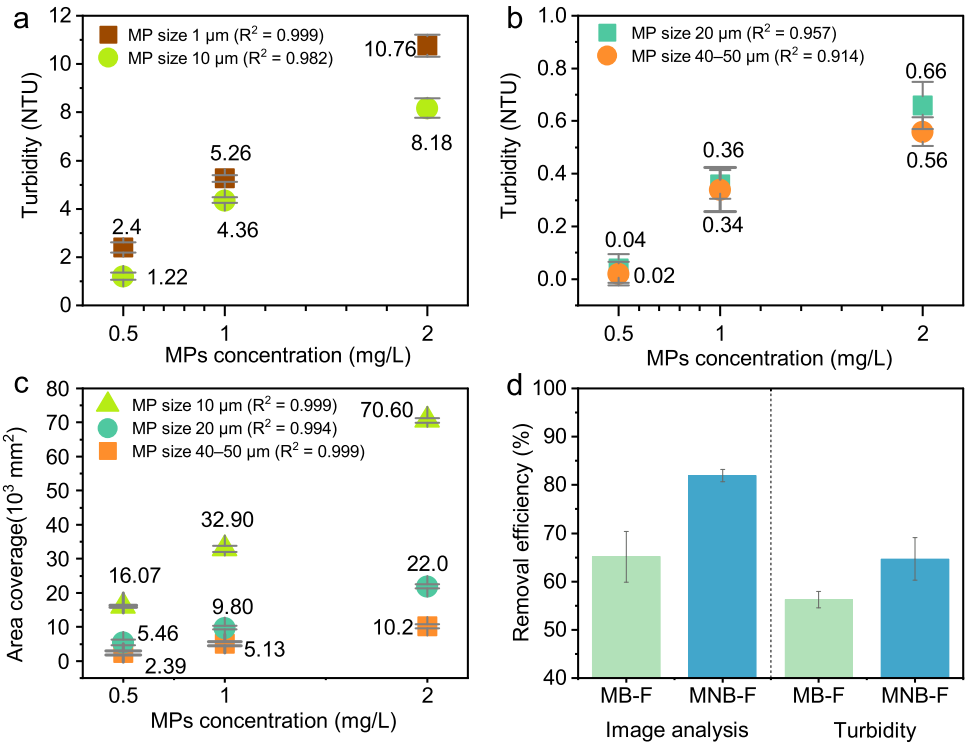

Fig. 4 | Comparative analysis of two MP quantification methods. a Turbidity calibration for MPs of 1 μm and 10 μm MPs. Data points and error bars represent the mean and standard deviation of five independent measurements. **b** Turbidity calibration for 20 μm and 40 μm MPs. Data points and error bars represent the mean and standard deviation of five independent measurements. **c** Calibration of the image analysis method for different-sized MPs. Data points and error bars represent the mean and standard deviation of two independent measurements. **d** Comparison of two quantification methods assessing the simultaneous removal of a mixture of MPs in four sizes with an $AlCl_3$ dosage of 10 ppm. Data points and error bars for turbidity tests represent the mean and standard deviation of five independent measurements each from two independent experiments; for the image analysis method, they represent the mean and standard deviation from two independent experiments.

types of wastewaters[50,51]. The three dosages selected in this study were based on a preliminary optimization study, where $AlCl_3$ dosages of 0–60 ppm were tested. The result indicated that omitting the coagulant or overdosing on the coagulant (>40 ppm) resulted in minimal MPs removal (<30%), as also suggested in previous research[52].

From the results, the removal efficiency increased with coagulant dosages and decreased with MPs sizes for both MB-F and MNB-F, with the lowest removal found for 1 μm MPs at 5 ppm $AlCl_3$, and the highest removal found for 40–50 μm MPs at 25 ppm $AlCl_3$. The removal efficiencies of MB-F and MNB-F showed comparable results for MPs sized 40–50 μm and 20 μm. High removal of MPs over 20 μm was also observed in previous studies, where the removal by MB-F can typically achieve over 80–90% (Supplementary Table 1). The high removal of larger MPs by both MB-F and MNB-F indicates that the effect of NBs is insignificant (independent *t*-test, $p > 0.05$) when the particle size is close to that of the MBs generated during MB-F, which already allows good collision and attachment efficiencies. However, for smaller-sized MPs (10 μm and 1 μm), MB-F exhibited a significant reduction in removal efficiency, particularly at lower coagulant dosages. The differences in removal efficiency between MB-F and MNB-F became more pronounced, as evidenced by the independent *t*-test ($p < 0.05$). MNB-F demonstrated over 10% improvement in removal efficiency compared to MB-F at both 10 ppm and 25 ppm dosages for 10 μm MPs, and a 12.4% improvement at a 10 ppm dosage for 1 μm MPs. MNB-F's enhanced MP removal efficiency demonstrated that it can achieve similar removal rates at lower dosages than MB-F, further suggesting a reduction in coagulant usage.

As collision and adhesion efficiencies between bubbles and particles are the key factors in determining flotation efficiency, we employed established numerical flotation models to investigate how the presence of NBs affects bubble-particle interactions. Bubble collision efficiency was calculated based on Flint-Howarth, which is suitable for small particles (Eq. (4))[53]. The adhesion efficiency was calculated with Yoon-Luttrell potential flow conditions, valid for particles smaller than 100 μm and bubbles smaller than 1 mm (Eq. (5))[54,55]:

$$E_c = \frac{v_p}{v_p + v_b} \tag{4}$$

$$E_a = \frac{\sin^2(2\arctan\exp(\frac{-3v_B t_i}{d_P + d_B}))}{\sin^2 90} \tag{5}$$

where E_c is collision probability, E_a is adhesion probability, d_B is bubble radius (μm), d_P is particle diameter (μm), v_b is bubble terminal rising velocity (μm s^{-1}), v_p is particle terminal velocity (μm s^{-1}) and t_i (s) is the induction time calculated. The specific equation and parameter values used are given in Supplementary Table 2.

The model results presented in Fig. 6 suggest that collision and adhesion probabilities increase as bubble sizes decrease. For instance, in the case of 1 μm particles, the collision probability is nearly zero when the bubble radius varies from 20 to 100 μm. However, it can be enhanced to around 0.6 when the bubble size is reduced to 100 nm. This indicates that NBs, which undergo Brownian motion in water, experience more frequent and effective collisions with MP particles (Fig. 6a, c). The adhesion process introduces a parameter known as induction time (t_i), which describes the time required to form a stable particle-bubble bond. The induction time can be calculated based on the contact angle and particle sizes. Previous studies comparing macro bubbles and MBs have reported an apparent enhancement (3.5–6%) in the contact angle by MBs when in contact with oil[56]. Another study

https://doi.org/10.1038/s41467-024-53304-3

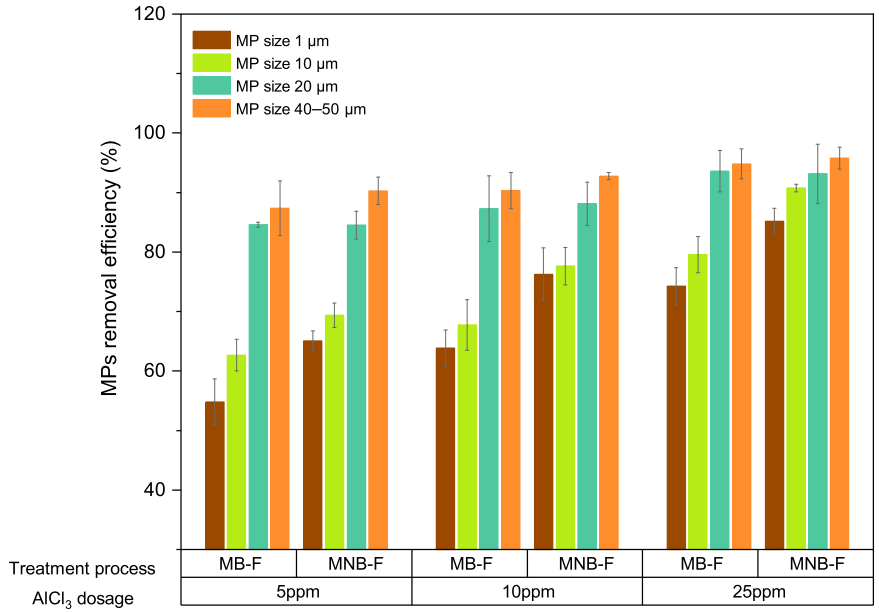

Fig. 5 | MP removal efficiency by MB-F and MNB-F. Comparison of removal efficiency for MPs of different sizes (1–50 μm) at different coagulant dosages by MB-F and MNB-F. Data points and error bars for 10, 20, and 40–50 μm MPs represent the mean and standard deviation from two independent experiments; for 1 μm MPs, they represent the mean and standard deviation of five independent measurements each from two independent experiments.

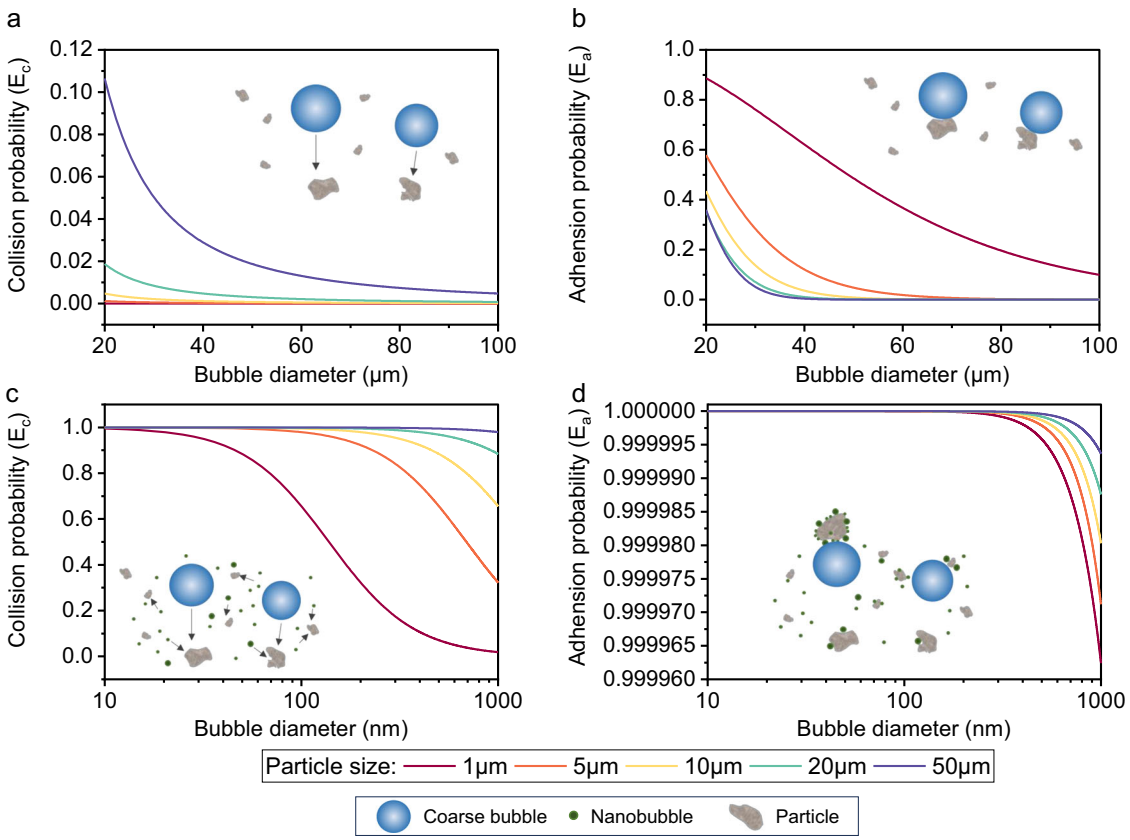

Fig. 6 | Conventional flotation model illustrating the effect of bubble size on collision and adhesion probabilities during the flotation process. a Collision probability between a bubble with a 20–100 μm radius and particles ranging from 1–50 μm in size. **b** Adhesion probabilities between a bubble with a 20–100 μm radius and particles ranging from 1–50 μm in size. **c** Collision probabilities between a bubble with a 0–1000 nm radius and particles ranging from 1–50 μm in size. **d** Adhesion probabilities between a bubble with a 0–1000 nm radius and particles ranging from 1–50 μm in size. Inset figures depict the collision (**a**, **c**) and adhesion (**b**, **d**) of particles and bubbles without (**a**, **b**) and with (**c**, **d**) the presence of NBs.

https://doi.org/10.1038/s41467-024-53304-3

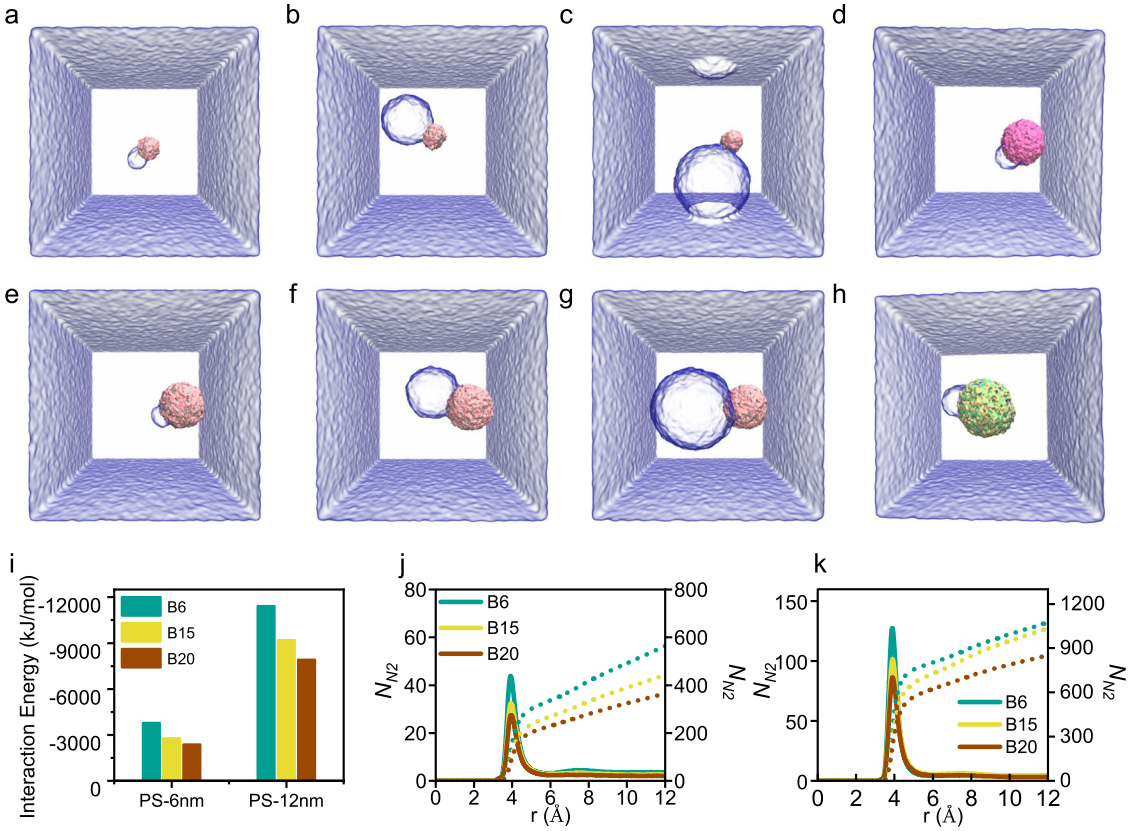

Fig. 7 | Molecular dynamic simulation of the interaction between NBs and NPs. The final equilibrium attachment states for **a** PS6B6, **b** PS6B15, **c** PS6B20, **d** PE12B6 **e** PS12B6, **f** PS12B15, **g** PS12B20, and **h** PET12B6. The water and NPs are shown as transparent and opaque surfaces, respectively, while N_2 molecules are not shown for clarity. **i** Interaction energy between NBs and NPs with respect to different sizes and NP composition. **j** Local (left, line) and cumulative (right, dot) distribution profiles between a 6 nm NP and N_2 NBs of various sizes. **k** Local (left, line) and cumulative (right, dot) distribution profiles between a 12 nm NP and N_2 NBs of different sizes.

found that droplets with NBs can enhance the contact angle by 8° compared to droplets without NBs when in contact with a graphite surface[57]. Therefore, we assumed a higher contact angle (8°) for the NBs' adhesion process when implementing the model. While collision probability exhibited significant variations with changes in bubble size, adhesion probability was found to be less sensitive to bubble radius. Regardless, a higher adhesion probability (approximately 1 in the nanometer range) was observed for NBs than for MBs (Fig. 6b, d). Overall, the model results suggest that the enhanced removal of sub-10 μm MPs can be attributed to the improved collision and adhesion between the bubbles and particles.

While conventional flotation models can provide insights into how NBs interact with particles during flotation, they are less frequently used to describe NBs than macro or microbubbles due to NBs' unique properties. MD simulation has emerged as a powerful tool for elucidating the physics and chemistry governing nanoscale phenomena. Recently, an increasing number of studies have begun employing MD simulations in NB research to gain a deeper understanding of the behavior of these nano-sized bubbles from a nanoscopic perspective. Due to computational limitations, most studies simulate NBs smaller than 10 nm, typically composed of nitrogen, argon, or oxygen gas[58–61].

In our analysis, we chose three bubble sizes (6, 15, and 20 nm, denoted as B6, B15, and B20) and two plastic sizes (6 and 12 nm) to simulate the interactions between smaller and larger bubbles and their effects on different-sized nanoplastics (NPs). The final equilibrium states of PS NPs and NBs are illustrated in Fig. 7a–c, e–g. The simulation results showed that NBs could spontaneously attach to NPs because of their hydrophobic nature, and the capillary bridge was formed as bubbles and particles approached each other (Supplementary Movies 1 and 2). We further calculated the interaction energy between NPs and NBs to explain the adhesion probability between a PS NP and an NB. As shown in Fig. 7i, the interaction energy between PS NPs and NBs decreases with increasing NB size for both large (PS6) and small (PS12) sized plastics and increases with particle sizes. This trend aligns with the predictions of theoretical models, revealing that an increase in NB size decreases the adhesion probability for both large and small PS NPs. To better understand the mechanisms responsible for the increased interaction strength between smaller bubbles and PS NPs, we gathered the local distributions of N_2 molecules around PS particles with different sizes, as shown in Fig. 7j, k. We also integrated the local N_2 distribution profiles to obtain the cumulative number of N_2 molecules residing at a specific distance around the PS particles. Since N_2 molecules do not interact with PS outside the cutoff of 1.2 nm in distance, we only considered the distribution of N_2 molecules within 1.2 nm around the PS particles. As shown in Fig. 7j, k, N_2 molecules interacted strongest with PS particles at a distance of 3.95 Å, regardless of the bubble size. In addition, NBs of smaller sizes exhibit stronger interactions with PS, as evidenced by higher peaks in local number distribution profiles. As indicated in cumulative number profiles, smaller NBs, having larger curvatures provided more N_2 molecules to interact with PS at specific distances, leading to stronger interactions.

In addition to freely suspended MP particles, a considerable number of particles are entrapped or occluded within the formed flocs during flotation. The size and density of these flocs are crucial factors in determining removal efficiency. Monitoring the flocs formed under three different dosages of $AlCl_3$ using a microscope and a laser beam (Supplementary Fig. 5a–c) revealed that increasing the dosage from 5 to 25 ppm led to an increase in both the sizes and

the densities of the flocs. The floc size distribution is described in Supplementary Fig. 6. When comparing the flotation of particles and flocs at the three dosages, it was evident that a denser layer of flocs was formed at the surface during MNB-F than MB-F (Supplementary Fig. 5d–f), which could be attributed to two factors. Firstly, MNB-F enhances the flotation of small flocs that are difficult to float with MBs alone by effectively capturing and removing those minuscule flocs, thereby boosting overall removal efficiency. Secondly, the high stability and hydrophobicity of NBs ensure their prolonged retention on the hydrophobic surfaces of particles. The extended retention can enhance the stability and strength of hydrophobic aggregates, thereby improving the flotation efficiency of MPs. These findings underscore the advantageous role of NBs in facilitating the successful flotation of entrapped MPs and promoting the formation of hydrophobic aggregates, the combined effect of which enhances overall flotation efficiency.

Building on this demonstration of NBs' positive effect on the removal of spherical PS MPs, we expanded the investigation to include irregular-shaped MPs smaller than 10 μm, comprised of three different polymer types, PS, polyethylene (PE), and polyethylene terephthalate (PET), and examined their removal by MB-F and MNB-F processes. The results indicated that the removal efficiencies for irregular-shaped PS and PE were comparable, whereas those for PET were notably lower. In the flotation process, density is the primary determinant of removal efficiency for different polymer types. Particles with higher densities tend to settle more readily, posing challenges for removal via flotation[62]. Consequently, the removal efficiencies for PS and PE, whose respective densities are 0.88–1.03 g cm^{-3} and 0.96–1.05 g cm^{-3}, were similar and higher compared to PET, which has a density of 1.38 g cm^{-3} (Supplementary Fig. 7). In addition, MD simulations also indicate that the interaction energy between a PS and a NB is comparable with that between a PE and a NB and stronger than that between a PET and a NB, which also explains the less effective removal of PET compared to PS and PE (Fig. 7d, h and Supplementary Fig. 8).

Furthermore, irregular-shaped MPs generally exhibited higher removal efficiencies than spherical MPs. The edges and corners of irregular particles could facilitate the thinning and rupture of the liquid film between the bubble and particle, thus reducing the critical induction time for particle capture and enhancing their collision efficiency with the bubbles[63,64]. A previous study comparing the removal of spherical and non-spherical PE MPs sized 50–60 μm via MB-F reported removal efficiencies of approximately 83–90% for irregularly shaped MPs, compared to about 52–53% for spherical MPs[62]. In our study, spherical PS and irregular PS did not show significant variations in their removal efficiencies, which may be attributed to differences in plastic sizes. The spherical MPs were consistently measured at 1 μm, whereas the irregular PS consisted of a mixture of particles smaller than 10 μm, with a large percentage being smaller than 1 μm. Additionally, since the irregular-shaped MPs were only available in white/transparent colors, a higher MP concentration (4 mg L^{-1}) was utilized than the tests for spherical particles (1 mg L^{-1}). This adjustment, which potentially influenced the comparative results, was necessary to ensure that the turbidity meter accurately reflected the concentration. Future studies should further explore these aspects to elucidate the dynamics of MPs removal across different shapes and polymer types. However, regardless of the MPs' polymer types and shapes, we observed an apparent enhancement in removal efficiency using the MNB-F process, suggesting a positive effect of the NBs in the flotation process.

Free radical detection and synergistic removal of organic matter during flotation

Radical generation by NBs is a widely debated topic within NB research, particularly regarding their potential to degrade pollutants through radical generation[18]. Given the growing interest in this potential, we conducted experiments to assess whether NBs could generate radicals in our system and explore how their addition during flotation processes might enhance the removal of organic substances.

Radical generation by NBs was tested using three commonly applied detection methods: Electron Paramagnetic Resonance (EPR) spectroscopy with DMPO as the spin trapping agent, High-Performance Liquid Chromatography (HPLC) with salicylic acid as the scavenger, and the fluorescence probe method using aminophenyl fluorescein (APF)[65,66]. While the EPR and HPLC methods failed to show a clear sign of radical presence in NB water (not reported in this work), possibly due to concentrations below the detection limit[67], the APF method, validated with a hydrogen peroxide (H_2O_2) calibration test (Supplementary Fig. 9), displayed an •OH peak at an emission wavelength of 515 nm. This was contrasted with DI water, which served as a negative control and showed no peak (Fig. 8a). Yet, a recent study suggested that the peak might be a false response, preventing a definitive conclusion about radical generation by NBs in the ambient condition[68]. We further investigated the in situ degradation of methylene blue during continuous NB generation. Figure 8b displays an apparent reduction in UV-Vis absorbance at 660 nm over 90 min, with 66.7% of the methylene blue degraded. The notably high degradation rate can also be attributed to H_2O_2 production during NB generation via the hydrodynamic cavitation method[69,70].

To investigate the simultaneous removal of organic compounds from synthetic wastewater, we measured the TOC of the wastewater before and after treatment with MB-F and MNB-F at varying dosages of coagulant (0, 5, 10, 25 ppm). When no coagulant was added, the reduction of TOC by MB-F and MNB-F showed no substantial difference (independent t-test, $p > 0.05$), suggesting minimal direct pollutant degradation by NBs. In other words, the removal was due to dilution by bubble-enriched water. When coagulant was added, MNB-F showed a clearer enhancement (2.5–7.2%) in TOC removal at all dosages (independent t-test, $p < 0.05$) (Fig. 8c). Given the minimal effect of direct radical degradation, the main reason behind the enhanced TOC removal by MNB-F when coagulant is present can be attributed to the higher flotation efficiency for small-sized organic flocs due to NBs.

Implementing NBs for MP removal in real wastewater

We further evaluated the removal of a mixture of four differently sized spherical PS MPs in real wastewater using MB-F and MNB-F. Due to the unknown concentration of naturally occurring MPs in the wastewater, we spiked the samples with equal concentrations of MPs to facilitate a meaningful comparison. The efficiency of MPs removal was determined by measuring the changes in turbidity, as the color of wastewater can interfere with the accuracy of results obtained through image analysis methods. The results obtained, as shown in Fig. 8d, indicated that the MB-F process achieved a removal efficiency of approximately 73.1%, while the MNB-F process exhibited a significantly higher removal efficiency of 87.4%, representing a 14.3% enhancement. In terms of TOC reduction, the initial concentration of TOC in the wastewater was approximately 278.91 mg L^{-1}, and the MB-F and MNB-F processes demonstrated TOC removal efficiencies of 27.9% and 38.5%, respectively. Notably, while no statistically significant difference in turbidity removal was observed between the two processes for synthetic wastewater (Fig. 4d), a clear disparity in turbidity removal was evident with real wastewater. This disparity can be attributed to the higher turbidity in real wastewater, where the MNB-F process enhances the removal of suspended particles in addition to artificially spiked MPs. These findings suggest that the MNB-F process is not hindered by the complex water matrices typical of real wastewater and successfully enhances the removal of MPs and other suspended particles.

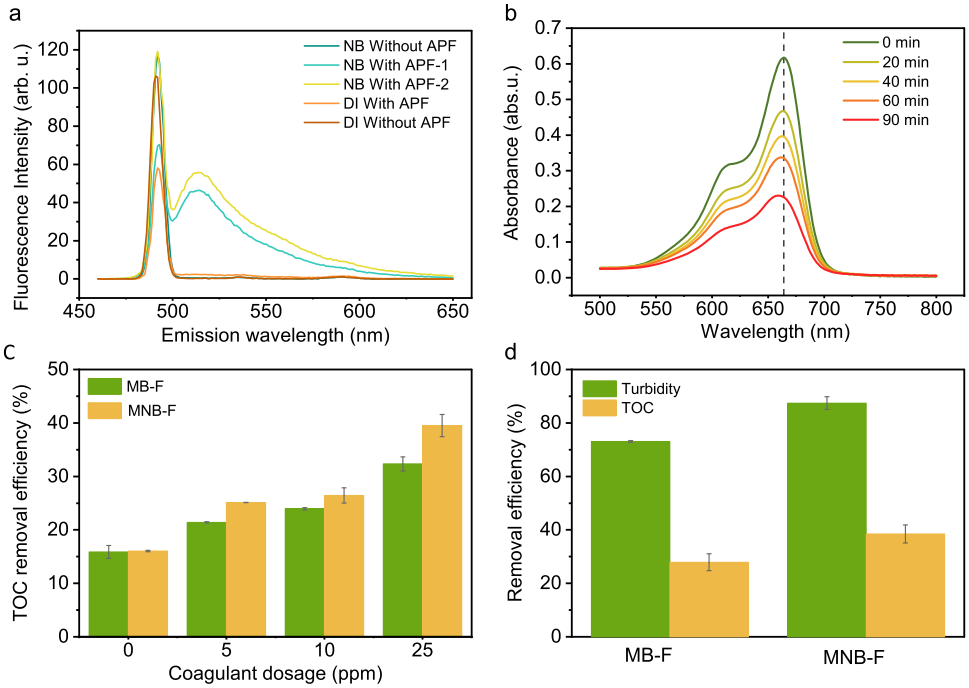

Fig. 8 | Assessment of NBs' reactivity in water. a Identification of hydroxyl radicals using the APF method; **b** In situ methylene blue degradation during NB generation; **c** Comparison of TOC removal by MB-F and MNB-F at coagulant dosages of 5, 10, 25 ppm (independent *t*-test, $p < 0.05$). **d** The removal of turbidity and TOC from the real wastewater by the two flotation processes at an $AlCl_3$ dosage of 10 ppm. Data points and error bars in **c** and **d** represent the mean and standard deviation of three independent measurements each from two independent experiments.

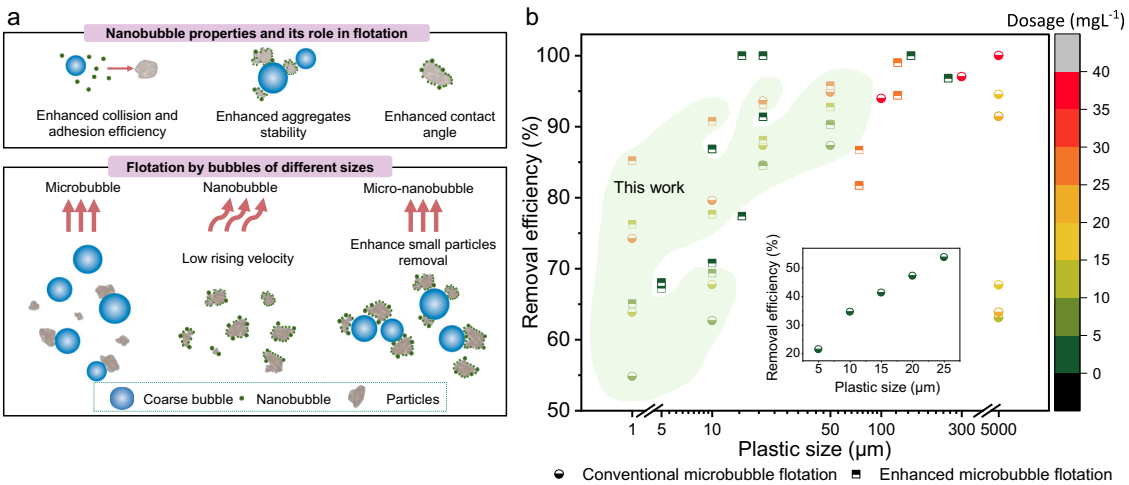

Fig. 9 | Demonstration of the mechanism and performance of NB-assisted flotation. a Schematic overview of NBs' properties and the flotation mechanisms by MB-F, NB-F, and MNB-F. **b** Comparison between our study and existing studies using conventional and enhanced microbubble flotation processes to remove MPs (data acquisition is described in Supplementary Note 1). Green shadow covers data points reported in this work. The inset figure displays data points in a lower removal efficiency range (20–50%).

Environmental impacts and mechanistic insights into the use of NBs in flotation

The observed enhancement in MPs removal efficiency and TOC removal during MNB-F can be attributed to several mechanisms, which have been supported by empirical evidence and theoretical models (Fig. 9a). Firstly, the small size of NBs plays a crucial role in increasing the collision and adhesion probabilities with particles, especially sub-10 μm MPs. Due to their small size and high concentrations, NBs exhibit Brownian motion in water, resulting in more frequent and efficient collisions and attachment with small-sized MPs. However, the small size of NBs also results in a lower rising velocity, which challenges their effective separation from the water. A combination of NBs and coarse bubbles is required to address this limitation. The coarse bubbles can provide the necessary buoyancy and upward transportation force to facilitate the flotation of attached particles to the water surface[71]. This synergistic effect between NBs and MBs ensures the efficient removal of the attached MPs. Secondly, the hydrophobic nature of NBs enables them to engage in hydrophobic interactions with particles. This interaction enhances the contact angle between bubbles, MPs and flocs, promoting greater adhesion and aggregation. Furthermore, the hydrophobic aggregates formed between NBs and particles exhibit long-

term stability, ensuring their persistence throughout the flotation process.

In striving to understand how bubble and particle sizes would affect their interactions, two simulations were conducted using conventional flotation models and MD. The conventional flotation model indicated that NBs could enhance the collision and adhesion probabilities with particles, and MD results showed that smaller bubbles can have greater interaction energy with particles at the nanoscale. While these results provide insights into how NBs might behave dynamically, computational and equipment limitations make it difficult to directly observe the interactions between the bubbles and particles, leaving a gap between modeling and experimentation that highlights the need for further research. Additionally, the enhanced flotation of flocs facilitated by NBs contributes to the removal of organic matter from wastewater. While NBs are considered reactive in water, the role of radicals generated by NBs is deemed minimal in this context, emphasizing the predominant influence of physical interactions rather than chemical reactions by NBs during flotation. The findings of this study underscore the critical role of NBs in conjunction with MBs in enhancing the removal efficiency for small-size MPs. This enhancement offers promising implications for the broader application of this technique in eliminating other fine suspended particles commonly found in wastewater.

For comparison, we summarized the MPs removal efficiencies reported in existing studies that investigated both conventional and enhanced flotation methods alongside our own (Fig. 9b). Compared with existing literature, our research bridges a critical gap by focusing on removing smaller-sized MPs, an area less explored in previous studies. Furthermore, our findings offer a robust strategy that not only boosts MP removal efficiency but achieves this with a relatively low use of coagulants.

While the practical implementation of NBs presents a viable path forward, one concern would be the feasibility of replacing existing techniques with NBs technology. Our preliminary economic assessment comparing the estimated costs of MB-F and MNB-F, published in a previous study, revealed that while the initial investment costs for MNB-F are higher than those for MB-F due to higher capital costs, the operational costs are 20% lower, as MNB-F reduces electricity consumption and chemical requirements[18]. Hence, it was projected that after 1 year of operation, the overall costs of MNB-F will become lower than those of MB-F. However, more studies are necessary to provide a more comprehensive economic assessment of NB technology implementation.

In summary, to overcome the limitations of flotation in efficiently eliminating small-sized MPs, which pose significant environmental threats, the present investigation explored the potential of MNB-F as a promising treatment process for the enhanced removal of these small particles. First, an analysis of MPs concentrations in treated wastewater was performed to provide an overview of the prevalence of small-sized MPs in wastewater and the challenges faced by conventional processes. To tackle the problem, MNB-F, a process combining NBs with MB-F, was compared with conventional MB-F and NB-F in terms of their MPs removal capabilities. The results revealed that while MB-F effectively eliminated particles larger than 20 μm, it was less effective at addressing MPs sized 10 μm and 1 μm. In comparison, the application of MNB-F exhibited a substantial enhancement in removing a mixture of different-sized MPs, improving removal rates by a maximum of 16.8% in synthetic wastewater and 14.3% in real wastewater, respectively. Flotation modeling revealed that the observed enhancement in MPs removal by MNB-F can be attributed to the addition of NBs, which increased the collision and adhesion efficiencies with particles. Furthermore, the attachment of NBs onto the surfaces of MP particles and flocs through hydrophobic interactions facilitated the formation of aggregates, thereby further enhancing the interaction with larger bubbles. Also, the utilization of MNB-F concurrently led to a 7.2% increase in the removal of organic matter in synthetic wastewater and 10.6% in real wastewater, likely attributable to the augmented flotation of organic flocs, albeit with minimal direct degradation of TOC through the NB-generated radicals. These findings serve as compelling proof of concept for utilizing the MNB-F technique as an innovative approach in water treatment processes, explicitly targeting removing small-sized particles.

Methods

Materials and chemicals

Spherical PS microbeads of different sizes (1 μm, 10 μm, 20 μm, and 40–50 μm) in various colors were purchased from Baseline (China). Irregular PS, PE, and PET particles were purchased from Hongfu Plastic (China). The microbeads were prepared as a stock solution (1 mg mL^{-1}) and subjected to 15 min of ultrasonication to ensure even dispersion before use. Sodium chloride (AR, 99.5%) and calcium chloride (99%) were purchased from Macklin Biochemical Co., Ltd (China). Glucose (≥99.5%), $AlCl_3{\cdot}6H_2O$ (99%), and H_2O_2 (30%) were purchased from Sigma-Aldrich (U.S.A). 3′-p-(aminophenyl) fluorescein (APF, ≥95%) was purchased from Maokang Biotechnology Co., Ltd (China). Real wastewater, obtained after chemically enhanced primary treatment, was obtained from Siu Ho Wan Sewage Treatment Work in Hong Kong. The characteristics of real wastewater are presented in Supplementary Table 3.

MPs characterization in real wastewater

Two liters of treated wastewater were obtained through bulk sampling from the effluent of a chemically enhanced primary treatment plant at Siu Ho Wan Sewage Treatment Works. Three 100 mL sub-samples were taken and digested with H_2O_2 to remove organics. Each sample was first filtered through a stainless-steel sieve (Ø = 5 μm), and MPs larger than 5 μm were characterized with a Renishaw via a confocal Raman microscope (Wotton-under Edge, U.K.). Subsequently, the solutions were further filtered using a gold-coated polycarbonate filter (Ø = 800 nm; Sterlitech, U.S.A.) and examined with an O-PTIR spectroscopy system (mIRage microspectroscope, Photothermal Spectroscopy Corp., U.S.A), which combines O-PTIR and Raman spectroscopy, to quantify particles between 1–5 μm in size. Specifically, following a typical procedure for MPs quantification by mIRage, four areas on the sieve were randomly selected and scanned, with each area representing 5.09% of the sieved area[72]. The average number of MPs was estimated by extrapolating the number of MPs observed in each scanned area to the total filter area.

Bench scale flotation process set-up

A schematic of the bench-scale system used in this study for MNB-F and MB-F is shown in Fig. 10. The system consisted of a compressed air supply line, a 2 L saturator vessel, a dissolved air distributor, and four units of 2 L jars (Aquagenics Pty Ltd, Australia). The prepared synthetic wastewater contained 5 mg L^{-1} of glucose, 100 mg L^{-1} of sodium chloride, and 50 mg L^{-1} of calcium chloride. Real wastewater was filtered through an 8 μm filter paper to remove large, suspended particles before use. To assess the removal of individual-sized MPs, a concentration of 1 mg L^{-1} of MPs was spiked in each jar tester. For measuring the removal of a mixture of MPs, a concentration of 1 mg L^{-1} per size type of MPs was spiked in each jar tester. For measuring the removal of irregular-shaped PS, PE, and PET, a concentration of 4 mg L^{-1} was used.

The designated amount of $AlCl_3$ was then dosed inside the jar testers, followed by 1 min of rapid mixing at 300 rpm, subsequent slow mixing at 30 rpm for 15 min, and finally, an injection of air-saturated water into the jar testers. Three coagulant dosages were chosen for the coagulation step: 5 ppm, 10 ppm, and 25 ppm. The 10 ppm and 25 ppm dosages were selected based on the commonly used range of coagulant dosage in flotation processes, while 5 ppm was tested in this study

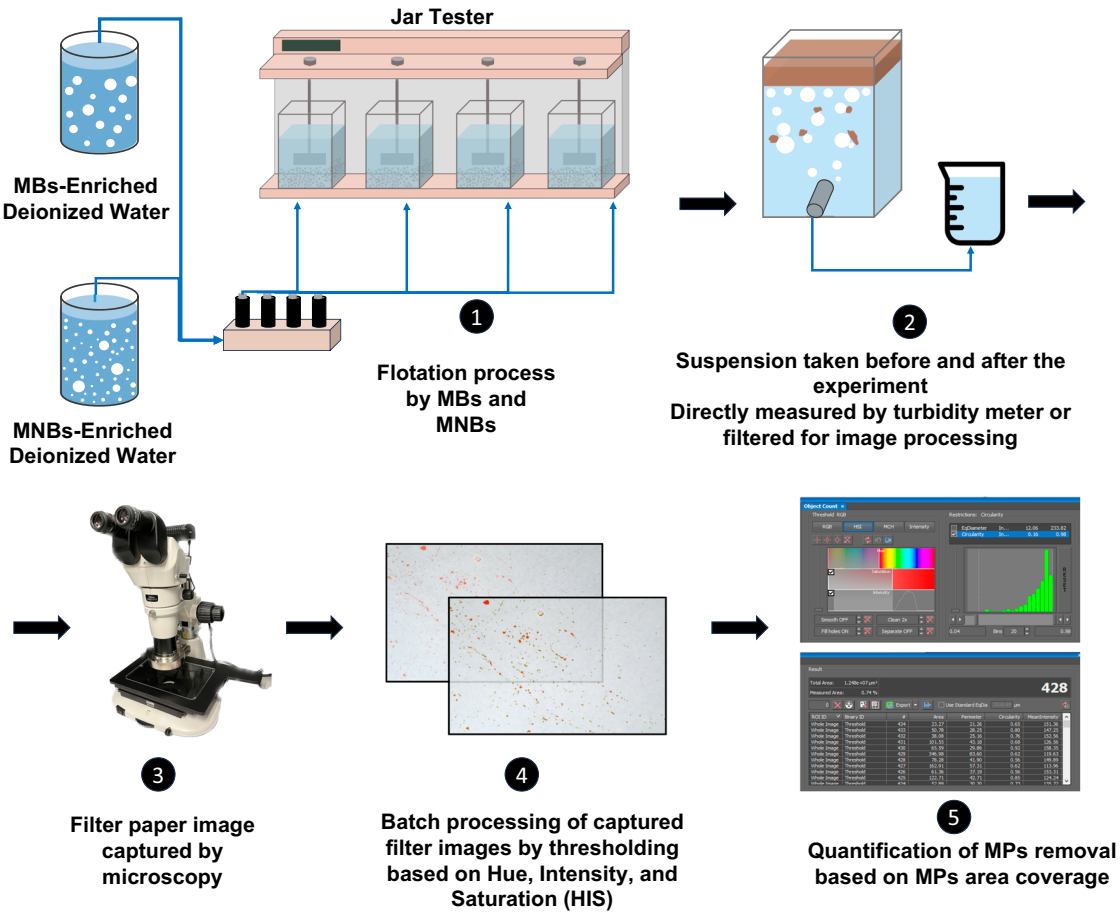

Fig. 10 | Experimental set-up of the study. The schematic of the flotation system and quantification of MPs using the image analysis method.

to determine the effectiveness of MNB-F at a low coagulant concentration[51]. During the MB-F process, the MBs water was generated by pressurizing a 2 L saturator at approximately 4–5 bar for 90 s, and the water was purged into the jar tester at a flow rate of 240–300 mL min^{-1}. The recycle ratio, which refers to the amount of air-saturated water added into the jar tester, was set to 20%, corresponding to adding 400 mL of air-saturated water into 1.6 L of the initial volume in the jar. For the MNB-F process, the MNB generator (aQua+ 075MO, AquaPro Solutions Pte Ltd, Singapore) was operated at an internal pump pressure of 3.8–4 bar for 15 min of continuous water recycling and generation in a 12 L tank. For NB-flotation, the generated MNB-enriched water was set aside for 3 min for MBs to disappear and was then purged into the jar tester at the same flow rate. The properties of NB water, including size distribution, concentration, and zeta potential, were characterized using NanoSight LM-10HS (UK) and Zetasizer (ZEN3600 Zettaliter NanoZS, Malvern Instruments, UK).

MP removal quantification

To assess the available methods for quantifying MPs, which remains a challenge in environmental research[73], we compared the accuracy of turbidity, a commonly used quantification method, with the image analysis method and subsequently adopted both approaches in this study. For turbidity-based quantification, the turbidity of five 12 mL samples of the suspension was measured using a turbidity meter (Yuefeng, China) before and after flotation, and the average was calculated. The image analysis method was quantified as follows: 400 mL of the water samples were taken from the sample outlet before coagulation and 10 min after flotation, then the samples were filtered with a 0.8 μm filter paper. The filter paper was observed under optical microscopy (SMZ1270i, Nikon, Japan), and 20–60 photos were captured of each filter paper depending on the magnification, ranging from 1X to 4X zoom for different particle sizes. The images were then batch processed through macro command using the built-in image analysis tool, i.e., NIS-elements BR, which can distinguish the colored MPs on the filter membrane based on the RGB and compute the total area coverage.

Finally, the overall removal efficiency was calculated using the equations below based on the difference in the area coverage or turbidity of the MPs on the filter before and after flotation. To account for the effect of dilution on removal effects, a dilution factor was introduced when calculating the initial MP concentration:

$$\text{Initial MP concentration} = \frac{\text{Sum of MP area coverage or turbidity in the before sample} \times \text{Initial water volume}}{\text{Final water volume}} \quad (6)$$

Then, the overall removal efficiency was calculated as follows:

$$\text{Removal Rate}(\%) = \frac{\text{Intial MP concentration} - \text{Final MP concentration}}{\text{Initial MP concentration}} \times 100\% \quad (7)$$

Molecular dynamic simulation for nano-scale bubble-particle interaction

The coarse-grain (CG) MD simulations were conducted to study the interactions between NB (6, 15, and 20 nm) and NPs (NP 6 and 12 nm) with different polymer types (PS, PE, PET). The systems, composed of NPs, N_2 molecules, and water, utilized the MARTINI force field[74]. The strategy for mapping atomistic NPs into CG beads and the

corresponding force field parameters were taken from the previous studies[75,76]. The N_2 and water molecules were modeled using parameters optimized by Lin et al.[77,78] and classic MARTINI water beads, respectively. The force field parameters for different species atoms were obtained by Lorentz-Berthelot combining rules. The NPs were randomly generated by randomly dispersing short polymer chains in a large simulation box to form the initial model. The system then underwent energy minimization followed by a 20 ns relaxation at a high temperature of 600 K, and subsequently, the system was subjected to an annealing procedure from 600 K to 300 K to speed up the energy relaxation. Based on the obtained structure, a 100 ns production run was performed to obtain the equilibrium state of the NPs particles. These equilibrated NPs particles and N_2 NBs were then placed in a $40 \times 40 \times 40$ nm^3 box and solvated with classic MARTINI water molecules. Additional diffused N_2 molecules were also added to the simulation box to maintain the NB structure[77,79]. Further simulations were conducted to determine the local density of N_2 NBs and diffused N_2 gas. In the composite system, the NPs' size was controlled by the number of polymer chains and the NBs' size by the N_2 molecules. The composite system model was first subjected to an energy minimization process, followed by a 20 ns relaxation process and a 300 ns production run in the NVT ensemble. The trajectories for the last 100 ns were used for analysis. The temperature in each process was maintained at 300 K using a V-rescale thermostat[80], while the pressure was kept at 1 bar using Berendsen barostat[81] for the production run. Each system was named after the sizes and components of NBs and NPs (e.g., PS12B6 indicates PS with a 12 nm NP and a 6 nm NB). All simulations were performed using the GROMACS 5.1.4 package[82], and Visual Molecular Dynamics (VMD) software (version 1.9.4a53 (June 29, 2021)) was used to render all snapshots[83].

Analysis of NBs' reactivity and organic removal

NBs' reactivity in water was evaluated to explore their ability to generate free radicals and their potential role in removing organic pollutants during flotation. First, NBs' in situ reactivity in water was accessed using a colorimetric method with methylene blue, where color depletion indicates the oxidation of methylene blue[84]. The NBs were continuously generated inside a bucket containing 0.3 mg L^{-1} of methylene blue and 16 L of DI water for over 90 min, and samples were taken at different time intervals. A chiller was used to control the temperature at 22 degrees Celsius to prevent thermal degradation. The samples were measured using Ultraviolet-visible spectrophotometers (UV-Vis, UV-3600, Shimadzu, Japan) to determine the change in concentration over time.

Next, we tested the presence of hydroxyl radicals by detecting the generation of ·OH radicals in the NB-enriched water using APF, a fluorescence probe. The fluorescence intensity was measured using a fluorescence spectrophotometer (RF-5310pc, Shimadzu, Japan) at excitation and emission wavelengths of 490 nm and 515 nm, respectively, and a slit width of 5 nm. During the experiment, 2 µL of APF (5 mM) was added to 10 mL of DI water with and without NBs, and the fluorescence intensity was measured in triplicate. Each sample was filtered with a 0.22 µm filter. The simultaneous removal of organics in the synthetic wastewater during flotation was also measured in triplicate based on the TOC of the suspension before and after the flotation with TOC-L (Shimadzu, Japan). The samples were filtered with a 0.25 µm filter before measurement.

Data availability

Source data are provided with this paper.

References

1. Sun, J., Dai, X., Wang, Q., van Loosdrecht, M. C. M. & Ni, B. J. Microplastics in wastewater treatment plants: detection, occurrence and removal. *Water Res.* **152**, 21–37 (2019).
2. Leusch, F. D., Lu, H. C., Perera, K., Neale, P. A. & Ziajahromi, S. Analysis of the literature shows a remarkably consistent relationship between size and abundance of microplastics across different environmental matrices. *Environ. Pollut.* **319**, 120984 (2023).
3. Krishnan, R. Y. et al. Recent approaches and advanced wastewater treatment technologies for mitigating emerging microplastics contamination—a critical review. *Sci. Total Environ.* **858**, 159681 (2023).
4. Ugwu, K., Herrera, A. & Gómez, M. Microplastics in marine biota: a review. *Mar. Pollut. Bull.* **169**, 112540 (2021).
5. Atugoda, T. et al. Interactions between microplastics, pharmaceuticals and personal care products: implications for vector transport. *Environ. Int.* **149**, 106367 (2021).
6. Browne, M. A., Dissanayake, A., Galloway, T. S., Lowe, D. M. & Thompson, R. C. Ingested microscopic plastic translocates to the circulatory system of the mussel, Mytilus edulis (L.). *Environ. Sci. Technol.* **42**, 5026–5031 (2008).
7. Watts, A. J. R. et al. Uptake and retention of microplastics by the shore crab carcinus maenas. *Environ. Sci. Technol.* **48**, 8823–8830 (2014).
8. Talvitie, J., Mikola, A., Koistinen, A. & Setälä, O. Solutions to microplastic pollution—removal of microplastics from wastewater effluent with advanced wastewater treatment technologies. *Water Res.* **123**, 401–407 (2017).
9. Keerthana Devi, M. et al. Removal of nanoplastics in water treatment processes: a review. *Sci. Total Environ.* **845**, 157168 (2022).
10. Zhang, Y., Diehl, A., Lewandowski, A., Gopalakrishnan, K. & Baker, T. Removal efficiency of micro- and nanoplastics (180 nm–125 µm) during drinking water treatment. *Sci. Total Environ.* **720**, 137383 (2020).
11. Edzwald, J. K. Dissolved air flotation and me. *Water Res.* **44**, 2077–2106 (2010).
12. Kyzas, G. Z. & Matis, K. A. Flotation in water and wastewater treatment. *Processes* **6**, 116 (2018).
13. Monira, S. et al. Nano and microplastics occurrence in wastewater treatment plants: a comprehensive understanding of microplastics fragmentation and their removal. *Chemosphere* **334**, 139011 (2023).
14. Fornasiero, D. & Filippov, L. O. Innovations in the flotation of fine and coarse particles. *J. Phys. Conf. Ser.* **879**, 012002 (2017).
15. Wang, Y., Li, Y., Tian, L., Ju, L. & Liu, Y. The removal efficiency and mechanism of microplastic enhancement by positive modification dissolved air flotation. *Water Environ. Res.* **93**, 693–702 (2021).
16. Etchepare, R., Oliveira, H., Nicknig, M., Azevedo, A. & Rubio, J. Nanobubbles: generation using a multiphase pump, properties and features in flotation. *Min. Eng.* **112**, 19–26 (2017).
17. Han, M. Y., Kim, M. K. & Ahn, H. J. Effects of surface charge, microbubble size and particle size on removal efficiency of electroflotation. *Water Sci. Technol.* **53**, 127–132 (2006).
18. Jia, M. et al. Nanobubbles in water and wastewater treatment systems: small bubbles making big difference. *Water Res.* **245**, 120613 (2023).
19. Farid, M. U. et al. Nanobubble-assisted scaling inhibition in membrane distillation for the treatment of high-salinity brine. *Water Res.* **209**, 117954 (2022).
20. Farid, M. U. et al. Hybrid nanobubble-forward osmosis system for aquaculture wastewater treatment and reuse. *Chem. Eng. J.* **435**, 135164 (2022).
21. Chang, G. H. et al. Effect of nanobubbles on the flotation performance of oxidized coal. *ACS Omega* **5**, 20283–20290 (2020).
22. Rosa, A. F. & Rubio, J. On the role of nanobubbles in particle-bubble adhesion for the flotation of quartz and apatitic minerals. *Min. Eng.* **127**, 178–184 (2018).
23. Tang, Y. et al. Reducing arsenic toxicity using the interfacial oxygen nanobubble technology for sediment remediation. *Water Res.* **205**, 117657 (2021).

24. Tao, D. Role of bubble size in flotation of coarse and fine particles—a review. *Sep. Sci. Technol.* **39**, 741–760 (2004).
25. Wang, H. N. et al. Regulation of bubble size in flotation: a review. *J. Environ. Chem. Eng.* **8**, 104070 (2020).
26. Haarhoff, J. & Edzwald, J. K. Modelling of floc-bubble aggregate rise rates in dissolved air flotation. *Water Sci. Technol.* **43**, 175–184 (2001).
27. Calgaroto, S., Azevedo, A. & Rubio, J. Separation of amine-insoluble species by flotation with nano and microbubbles. *Min. Eng.* **89**, 24–29 (2016).
28. Etchepare, R., Oliveira, H., Azevedo, A. & Rubio, J. Separation of emulsified crude oil in saline water by dissolved air flotation with micro and nanobubbles. *Sep. Purif. Technol.* **186**, 326–332 (2017).
29. Calgaroto, S., Azevedo, A. & Rubio, J. Flotation of quartz particles assisted by nanobubbles. *Int. J. Min. Process* **137**, 64–70 (2015).
30. Carbery, M. et al. How small is the big problem? Small microplastics <300 µm abundant in marine surface waters of the Great Barrier Reef Marine Park. *Mar. Pollut. Bull.* **184**, 114179 (2022).
31. Wang, Z., Lin, T. & Chen, W. Occurrence and removal of microplastics in an advanced drinking water treatment plant (ADWTP). *Sci. Total Environ.* **700**, 134520 (2020).
32. Park, T. J. et al. Distributions of microplastics in surface water, fish, and sediment in the vicinity of a sewage treatment plant. *Water* **12**, 3333 (2020).
33. Uurasjärvi, E., Hartikainen, S., Setälä, O., Lehtiniemi, M. & Koistinen, A. Microplastic concentrations, size distribution, and polymer types in the surface waters of a northern European lake. *Water Environ. Res.* **92**, 149–156 (2020).
34. Tse, Y. T., Chan, S. M. N. & Sze, E. T. P. Quantitative assessment of full size microplastics in bottled and tap water samples in Hong Kong. *Int. J. Environ. Res. Public Health* **19**, 13432 (2022).
35. Enders, K., Lenz, R., Stedmon, C. A. & Nielsen, T. G. Abundance, size and polymer composition of marine microplastics ≥10 µm in the Atlantic Ocean and their modelled vertical distribution. *Mar. Pollut. Bull.* **100**, 70–81 (2015).
36. Samandra, S. et al. Quantifying environmental emissions of microplastics from urban rivers in Melbourne, Australia. *Mar. Pollut. Bull.* **189**, 114709 (2023).
37. Erni-Cassola, G., Gibson, M. I., Thompson, R. C. & Christie-Oleza, J. A. Lost, but found with Nile red: a novel method for detecting and quantifying small microplastics (1 mm to 20 µm) in environmental samples. *Environ. Sci. Technol.* **51**, 13641–13648 (2017).
38. Talvitie, J., Mikola, A., Setälä, O., Heinonen, M. & Koistinen, A. How well is microlitter purified from wastewater?—a detailed study on the stepwise removal of microlitter in a tertiary level wastewater treatment plant. *Water Res.* **109**, 164–172 (2017).
39. Magni, S. et al. The fate of microplastics in an Italian Wastewater Treatment Plant. *Sci. Total Environ.* **652**, 602–610 (2019).
40. Swart, B., Chew, Y. M. J. & Wenk, J. Simultaneous monitoring of flow patterns, and bubble, and plastics micro-particle characteristics in Dissolved Air Flotation (DAF). *Chem. Eng. Res. Des.* **197**, 148–158 (2023).
41. Gonzalez-Galvis, J. P. & Narbaitz, R. M. Large batch bench-scale dissolved air flotation system (LB-DAF) for drinking water treatability tests. *Environ. Sci.* **6**, 1791–1804 (2020).
42. Schmideder, S., Thurin, L., Kaur, G. & Briesen, H. Inline imaging reveals evolution of the size distribution and the concentration of microbubbles in dissolved air flotation. *Water Res.* **224**, 119027 (2022).
43. Nazari, S. et al. Study of effective parameters on generating submicron (nano)-bubbles using the hydrodynamic cavitation. *Physicochem. Probl. Miner. Process.* **56**, 884–904 (2020).
44. Nirmalkar, N., Pacek, A. W. & Barigou, M. On the existence and stability of bulk nanobubbles. *Langmuir* **34**, 10964–10973 (2018).
45. Zhou, W. G. et al. Electrokinetic potential reduction of fine particles induced by gas nucleation. *Ultrason. Sonochem.* **67**, 105167 (2020).
46. Parkinson, L., Sedev, R., Fornasiero, D. & Ralston, J. The terminal rise velocity of 10-100 µm diameter bubbles in water. *J. Colloid Interface Sci.* **322**, 168–172 (2008).
47. Amaya-Bower, L. & Lee, T. Single bubble rising dynamics for moderate Reynolds number using Lattice Boltzmann Method. *Comput. Fluids* **39**, 2405–2413 (2010).
48. Bayarkhuu, B. & Byun, J. Optimization of coagulation and sedimentation conditions by turbidity measurement for nano- and microplastic removal. *Chemosphere* **306**, 135572 (2022).
49. Lapointe, M., Farner, J. M., Hernandez, L. M. & Tufenkji, N. Understanding and improving microplastic removal during water treatment: impact of coagulation and flocculation. *Environ. Sci. Technol.* **54**, 8719–8727 (2020).
50. You, Z., Xu, H., Sun, Y., Zhang, S. & Zhang, L. Effective treatment of emulsified oil wastewater by the coagulation-flotation process. *RSC Adv.* **8**, 40639–40646 (2018).
51. Miranda, R., Latour, I. & Blanco, A. Understanding the efficiency of aluminum coagulants used in dissolved air flotation (DAF). *Front. Chem.* **8**, 27 (2020).
52. Esfandiari, A. & Mowla, D. Investigation of microplastic removal from greywater by coagulation and dissolved air flotation. *Process Saf. Environ. Prot.* **151**, 341–354 (2021).
53. Flint, L. R. & Howarth, W. J. The collision efficiency of small particles with spherical air bubbles. *Chem. Eng. Sci.* **26**, 1155–1168 (1971).
54. Yoon, R. H. & Luttrell, G. H. The effect of bubble size on fine particle flotation. *Miner. Process. Extr. Metal. Rev.* **5**, 101–122 (1989).
55. Kouachi, S., Bouhenguel, M., Amirech, A. & Bouchemma, A. Yoon-Luttrell collision and attachment models analysis in flotation and their application on general flotation kinetic model. *Desalination* **264**, 228–235 (2010).
56. Lim, M. W., Lau, E. V. & Poh, P. E. Analysis of attachment process of bubbles to high-density oil: influence of bubble size and water chemistry. *J. Taiwan Inst. Chem. Eng.* **68**, 192–45 (2016).
57. Ma, F. & Tao, D. A study of mechanisms of nanobubble-enhanced flotation of graphite. *Nanomaterials* **12**, 3361 (2022).
58. Feng, M. et al. How sodium chloride extends lifetime of bulk nanobubbles in water. *Soft Matter* **18**, 2968–2978 (2022).
59. Aluthgun Hewage, S. & Meegoda, J. N. Molecular dynamics simulation of bulk nanobubbles. *Colloids Surf. A Physicochem. Eng. Asp.* **650**, 129565 (2022).
60. Lu, Y. et al. Molecular simulations on the stability and dynamics of bulk nanobubbles in aqueous environments. *Phys. Chem. Chem. Phys.* **23**, 27533–27542 (2021).
61. Kadivar, E., Rajabpour, A. & El Moctar, O. Nanobubble collapse induced erosion near flexible and rigid boundaries: a molecular dynamics study. *Fluids* **8**, 154 (2023).
62. Swart, B., Pihlajamäki, A., John Chew, Y. M. & Wenk, J. Microbubble-microplastic interactions in batch air flotation. *Chem. Eng. J.* **449**, 137866 (2022).
63. Koh, P. T. L., Hao, F. P., Smith, L. K., Chau, T. T. & Bruckard, W. J. The effect of particle shape and hydrophobicity in flotation. *Int. J. Min. Process* **93**, 128–134 (2009).
64. Chen, Y., Zhuang, L. & Zhang, Z. Effect of particle shape on particle-bubble interaction behavior: a computational study using discrete element method. *Colloids Surf. A Physicochem. Eng. Asp.* **653**, 130003 (2022).
65. Liu, S., Oshita, S., Kawabata, S., Makino, Y. & Yoshimoto, T. Identification of ROS produced by nanobubbles and their positive and negative effects on vegetable seed germination. *Langmuir* **32**, 11295–11302 (2016).
66. Wang, W., Fan, W., Huo, M., Zhao, H. & Lu, Y. Hydroxyl radical generation and contaminant removal from water by the collapse of

microbubbles under different hydrochemical conditions. *Water Air Soil Pollut.* **229**, 86 (2018).
67. Zhang, Y., Fan, W., Li, X., Wang, W. X. & Liu, S. Enhanced removal of free radicals by aqueous hydrogen nanobubbles and their role in oxidative stress. *Environ. Sci. Technol.* **56**, 15096–15107 (2022).
68. Chae, S. H., Kim, M. S., Kim, J. H. & Fortner, J. D. Nanobubble reactivity: evaluating hydroxyl radical generation (or lack thereof) under ambient conditions. *ACS ES T Eng.* **3**, 1504–1510 (2023).
69. De-Nasri, S. J. et al. Quantifying OH radical generation in hydrodynamic cavitation via coumarin dosimetry: influence of operating parameters and cavitation devices. *Ultrason. Sonochem.* **90**, 106207 (2022).
70. Bandala, E. R. & Rodriguez-Narvaez, O. M. On the nature of hydrodynamic cavitation process and its application for the removal of water pollutants. *Air Soil Water Res.* **12**, 1–16 (2019).
71. Cihan, A. & Corapcioglu, M. Y. Effect of compressibility on the rise velocity of an air bubble in porous media. *Water Resour. Res.* **44**, W04409 (2008).
72. Lin, X., Gowen, A. A., Chen, S. & Xu, J. L. Baking releases microplastics from polyethylene terephthalate bakeware as detected by optical photothermal infrared and quantum cascade laser infrared. *Sci. Total Environ.* **924**, 171408 (2024).
73. Lamichhane, G. et al. Microplastics in environment: global concern, challenges, and controlling measures. *Int. J. Environ. Sci. Technol.* **20**, 4673–4694 (2023).
74. Marrink, S. J., Risselada, H. J., Yefimov, S., Tieleman, D. P. & De Vries, A. H. The MARTINI force field: coarse grained model for biomolecular simulations. *J. Phys. Chem. B* **111**, 7812–7824 (2007).
75. Li, L. et al. Distinguishing the nanoplastic-cell membrane interface by polymer type and aging properties: translocation, transformation and perturbation. *Environ. Sci. Nano* **10**, 440–453 (2022).
76. Rossi, G., Monticelli, L., Puisto, S. R., Vattulainen, I. & Ala-Nissila, T. Coarse-graining polymers with the MARTINI force-field: polystyrene as a benchmark case. *Soft Matter* **7**, 698–708 (2011).
77. Lin, X., Tian, F. & Marrink S.-J. Martini coarse-grained nitrogen gas model for lipid nanobubble simulations. *ChemRxiv* https://doi.org/10.26434/chemrxiv.13591283.v2 (2021).
78. Gao, Z., Wu, W. X., Sun, W. T. & Wang, B. Understanding the stabilization of a bulk nanobubble: a molecular dynamics analysis. *Langmuir* **37**, 11281–11291 (2021).
79. Zhang, M., Tu, Y. S. & Fang, H. P. Concentration of nitrogen molecules needed by nitrogen nanobubbles existing in bulk water. *Appl. Math. Mech.* **34**, 1433–1438 (2013).
80. Bussi, G., Donadio, D. & Parrinello, M. Canonical sampling through velocity rescaling. *J. Chem. Phys.* **126**, 014101 (2007).
81. Berendsen, H. J. C., Postma, J. P. M., Van Gunsteren, W. F., Dinola, A. & Haak, J. R. Molecular dynamics with coupling to an external bath. *J. Chem. Phys.* **81**, 3684–3690 (1984).
82. Abraham, M. J. et al. Gromacs: high performance molecular simulations through multi-level parallelism from laptops to supercomputers. *SoftwareX* **1–2**, 19–25 (2015).
83. Humphrey, W., Andrew, D. & Klaus, S. VMD: visual molecular dynamics. *J. Mol. Graph.* **14**, 33–38 (1996).
84. Westerhoff, P. K., Sinha, S. & Bi, Y. Quantification of nanobubble reactivity in water. (2021).
85. Rohatgi, A. WebPlotDigitizer. v. 4.8. apps.automeris.io/wpd4/ (2024).

Acknowledgements

This work was supported by ECF—Environmental and Conservation Fund (05/2020), and the Research Grants Council of the Hong Kong Special Administrative Region, China through (Project Nos. RFS2223-1S04, T21-604/19-R, 15307322, and R7003-21).

Author contributions

A.K.A., M.U.F., and M.J. conceived the research. A.K.A. and M.U.F. coordinated and supervised the research. M.J. and M.U.F. designed and carried out the experiments and analyzed data. Y.W.H. and J.F. contributed to bubble and plastic characterization. X.M. and J.F. contributed to the molecular dynamic simulation. P.W., M.B., and G.L. contributed to the characterization and discussion of data. M.J., Y.W.H., X.M., A.K.A., M.U.F., T.N., and Y.H. wrote and revised the manuscript.

Competing interests

The authors declare no competing interests.

Additional information

Supplementary information The online version contains supplementary material available at https://doi.org/10.1038/s41467-024-53304-3.

Correspondence and requests for materials should be addressed to Muhammad Usman Farid or Alicia Kyoungjin An.

Peer review information *Nature Communications* thanks Jannis Wenk and the other, anonymous, reviewer for their contribution to the peer review of this work. A peer review file is available.